The Supporting Information for Third-order Nonlinear Optical Properties and Absorption Spectra of The Host-guest Complexes formed between Fullerene and Cycloparaphenylene ([n]CPP: n= 9, 10 and 11)

Li Wang[*†], Yan-Li Liu[†], Quan-Jiang Li[†], Di He[†], Sheng-Hui Chen[†] and Mei-Shan Wang[*†‡]

[†]School of Physics and Optoelectronics Engineering, Ludong University, Yantai, 264025, Shandong, China.

[‡]School of Integrated Circuits, Ludong University, Yantai, 264025, Shandong, China.

E-mail: wangl@ldu.edu.cn (L. Wang); yanliliu@ldu.edu.cn (Y. L. Liu); quanjiangli@126.com (Q. J. Li); hedi@ldu.edu.cn (D. He); csh2010@163.com (S. H. Chen); mswang1971@163.com (M. S. Wang)

The calculation formulas of a series of indicators.

A series of indicators for the analysis of electron excitation characteristics based on density difference were performed at TD-DFT. The function of overlap between electron and hole distributions can be evaluated as:

$$S_r = \int S_r(r)dr = \int \sqrt{\rho^{hole}(r)\rho^{ele}(r)}dr \tag{6}$$

D index measures the distance between the hole and the electron's center of mass[1]:

$$D_x = |X_{ele} - X_{hole}| \quad D_y = |Y_{ele} - Y_{hole}| \quad D_z = |Z_{ele} - Z_{hole}|$$

$$D = \sqrt{(D_x)^2 + (D_y)^2 + (D_z)^2} \tag{7}$$

X_{hole} refers to the x-coordinate of the hole's center of mass, which can be obtained by integrating the ρ^{hole} function times the x-coordinate variable in full space. The so-called center of mass corresponds to the most central and representative point of the overall distribution of the function.

Another quantitative description of the distribution characteristics of holes and electrons in total space:

$$\sigma_{hole,x} = \sqrt{\int (x - X_{hole})^2 \rho^{hole}(r)dr}$$

$$\Delta\sigma = |\sigma_{ele}| - |\sigma_{hole}|$$

$$H = (|\sigma_{ele}| - |\sigma_{hole}|)/2$$

$$t = D - H_{CT}$$

$$HDI = 100 \times \sqrt{\int [\rho^{hole}(r)]^2 dr}$$

$$EDI = 100 \times \sqrt{\int [\rho^{ele}(r)]^2 dr}$$

$$E_c = \iint \frac{\rho^{hole}(r_1)\rho^{ele}(r_2)}{|r_1 - r_2|} dr_1 dr_2 \tag{8}$$

The σ index measures the overall distribution of holes, or electrons. Δσ measure the difference in the width of the spatial distribution of electrons and holes. H index reflects the overall average distribution width of electrons and holes. The t index measures the degree of hole and electron separation. t > 0 implies that the separation between the hole and the electron is relatively sufficient due to CT. t< 0 indicates that there is no significant separation between the hole and the electron. The HDI was hole delocalization index, EDI was electron delocalization index and E_c was exciton binding energy.

The detailed description of the Localized orbital locator (LOL) maps.

Localized orbital locator (LOL, Figure 1) maps are often used to explain structures and bonds in a clear and intuitive way. The limit possible values of LOL are: upper limit LOL = 1 for perfect localization, upper limit LOL = 0.5 for gas-like electron pairs, and lower limit LOL = 0 for non-bonding regions. To make the image sharper, we set the color ratio from 0.0 to 0.8. Thus, the pale green LOL basins (LOL=0.3~0.6) represent fast-moving electrons (delocalized electrons). The slowest electron region is yellowish red (LOL=0.6~0.8), which conforms to the typical two-electron/two-center bonding situation.

The detailed description of the transition density matrix (TDM).

Transition density matrix (TDM) between electronic state K and state L is denoted by P^{KL}, during excited state calculation in many quantum chemistry programs this matrix can be outputted in the form of expansion by atomic-center basis functions. We can further contract such matrix by following equation to make it represented by atom centers:

$$P_{A,B}^{KL} = \sum_{\mu \in A} \sum_{v \in B} (P_{\mu v}^{KL})^2$$

where μ and v denote the basis functions centered at atom A and on B respectively. Diagonal terms, e.g. $P_{A,B}^{KL}$, represents the magnitude of induced charge on atom A when the system undergoes electron transition from state K to L. While off-diagonal terms, e.g. $P_{A,B}^{KL}$, displays the strength of hole-electron coherence between atom A and B when electron transits. If this matrix is plotted as a color-filled map, then the primary atoms involved in specific electron transition mode, and the spatial span of the electron transition can be clearly and visually studied, this is especially useful for analyzing large-size and conjugated molecules. Commonly hydrogens can be omitted when plotting.

The detailed description of the charge density difference (CDD).

The the charge density difference (CDD) maps corresponding to the main excited states were carried out to analyze the electron transition patterns. The CDD was evaluated as:

$$\Delta\rho(r) = \rho^{ele}(r) - \rho^{hole}(r) \tag{6}$$

where $\rho^{ele}(r)$ and $\rho^{hole}(r)$ represented the electron and hole densities, respectively. Where, purple and blue parts were corresponded to the regions for accumulation and depletion of electron densities, respectively.

Table S1. The energy levels of HOMOs, LUMOs and the E_{gap} values of the single molecules C_{60}, Li+@C_{60}, [9-11]CPP at B3LYP/6-31G(d).

Complex	Functional	HMOM	LUMO	E_{gap}
C_{60}	B3LYP	-6.03	-3.14	2.89
	B3LYP-D3	-5.55	-3.38	2.17
Li+@C_{60}	B3LYP	-5.18	-1.71	3.47
	B3LYP-D3	-9.62	-6.72	2.90
[9]CPP	B3LYP	-5.15	-1.72	3.43
	B3LYP-D3	-5.10	-1.75	3.35
[10]CPP	B3LYP	-5.23	-1.66	3.57
	B3LYP-D3	-5.18	-1.69	3.49
[11]CPP	B3LYP	-5.23	-1.67	3.56
	B3LYP-D3	-5.18	-1.71	3.47

Table S2. The energy levels of HOMOs, LUMOs and the E_{gap} values of the single molecules C_{60}, Li+@C_{60}, [9-11]CPP and the complexes [9-11]CPP⊂C_{60}, [9-11]CPP⊂Li$^+$@C_{60} at B3LYP-D3/6-31G(d).

Complex	HMOM	LUMO	E_{gap}
C_{60}	-5.55	-3.38	2.17
Li$^+$@C_{60}	-9.62	-6.72	2.90
[9]CPP	-5.10	-1.75	3.35
[10]CPP	-5.18	-1.69	3.49
[11]CPP	-5.18	-1.71	3.47
[9]CPP⊂C_{60}	-5.10	-3.21	1.89
[10]CPP⊂C_{60}	-5.29	-3.06	2.23
[11]CPP⊂C_{60}	-5.31	-3.12	2.19
[9]CPP⊂Li$^+$@C_{60}	-7.15	-6.21	0.94
[10]CPP⊂Li$^+$@C_{60}	-7.20	-6.09	1.11
[11]CPP⊂Li$^+$@C_{60}	-6.99	-6.18	0.81

Table S3. The components of the total polarizability α (a.u.) for the studied complexes obtained by BhandHLYP/6-31+G(d) level.

Complex	α_{xx}	α_{yy}	α_{zz}	α_{tot}	$<R^2>$
C_{60}	536.9	536.9	536.9	536.9	17055.8
$Li^+@C_{60}$	523.8	523.8	523.8	523.8	17082.5
[9]CPP	825.4	807.8	512.5	715.2	52599.0
[10]CPP	918.8	918.5	569.5	802.3	71336.27
[11]CPP	1050.0	1027.4	625.8	901.1	94217.3
[9]CPP$\square$C$_{60}$	1231.4	1224.1	971.1	1142.2	76007.6
[10]CPP$\square$C$_{60}$	1350.8	1344.6	913.1	1202.8	87149.5
[11]CPP$\square$C$_{60}$	1512.3	1403.8	982.6	1299.6	110469.8
[9]CPP$\square$Li$^+$C$_{60}$	1250.3	1246.1	966.1	1154.2	75437.7
[10]CPP$\square$Li$^+$C$_{60}$	1380.1	1369.1	913.5	1220.9	87891.1
[11]CPP$\square$Li$^+$C$_{60}$	1561.4	1426.3	979.7	1322.5	110905.2

Table S4. The components of the second hyperpolarizabilities γ (a.u.) for the studied complexes obtained by BhandHLYP/6-31+G(d) level.

Complex	γ_{xxxx}	γ_{yyyy}	γ_{zzzz}	γ_{xxyy}	γ_{xxzz}	γ_{yyzz}	γ_{tot}
C_{60}	119952	119942	119915	39980.8	39987.9	39966.2	118353.0
$Li^+@C_{60}$	92712.8	92712.1	92705.7	30904.3	30901.2	30902.5	92709.3
[9]CPP	2049940.0	1834180.0	67293.9	652681.0	16583.6	17572.9	1065017.8
[10]CPP	2371840.0	2375590.0	74507.5	790854.0	16235.5	16128.5	1293674.7
[11]CPP	3360420.0	2986310.0	81896.8	1050830.0	15586.0	15966.9	1718678.5
[9]CPP□C_{60}	1119610.0	1116620.0	178745.0	369481	90840.9	88351.2	702464.2
[10]CPP□C_{60}	1236610.0	1225850.0	129359.0	406857	54153.2	55610.9	725012.2
[11]CPP□C_{60}	1969120.0	1378060.0	139169.0	501412	54614	58561.9	943105.0
[9]CPP□Li^+C_{60}	1358480.0	1390500.0	185250.0	462024	127535	140007	878672.4
[10]CPP□Li^+C_{60}	1627270.0	1727740.0	106394.0	505450	45413.1	48881.1	932178.5
[11]CPP□Li^+C_{60}	2762830.0	2166350.0	115271.0	719483	43235.3	53841.6	1335514.2

Table S5. Simulated wavelengths (λ, nm), energies (E_{ge}, eV), oscillator strengths (f_{os}) and major contributions for the complexes.

Complex	State	λ	E_{ge}	f_{os}	Excitation (% compositiosn)
[9]CPP$\subset$C$_{60}$	S38	325.0	3.82	0.599	H-1→L+3 (36%), H→L+7 (39%)
[10]CPP$\subset$C$_{60}$	S38	312.9	3.98	0.908	H→L+8 (32%), H-1→L+3 (13%) H-3→L+3 (11%)
[11]CPP$\subset$C$_{60}$	S39	307.0	4.04	1.392	H-2→L+6 (20%), H→L+7 (17%) H→L+8 (14%), H-2→L+3 (11%)
[9]CPP$\subset$Li$^+$@C$_{60}$	S32	340.7	3.64	0.560	H-1→L+6 (20%), H→L+3 (18%) H→L+5 (18%), H→L+7 (18%)
[10]CPP$\subset$Li$^+$@C$_{60}$	S44	323.2	3.84	0.798	H-8→L+1 (27%), H→L+8 (18%) H-1→L+6 (17%)
[11]CPP$\subset$Li$^+$@C$_{60}$	S44	324.3	3.82	1.217	H-1→L+6 (29%), H→L+8 (33%)

Table S6. The wavelength (λ), transition energy (E_{ge}) charge density difference (CDD), transition density matrix (TDM), overlap of hole-electron index (Sr), The distance between the hole and the electron's center of mass index (D), The overall mean distribution width of electrons and holes index (H), the degree of hole and electron separation index (t), hole delocalization index (HDI), electron delocalization index (EDI), exciton binding energy (E_c) of the excited state corresponding to the main absorption peak of C_{60}, [10]CPP and [10]CPP□C_{60}.
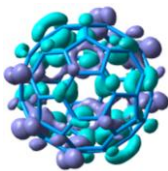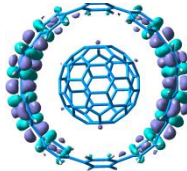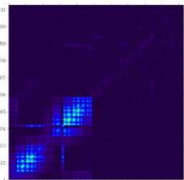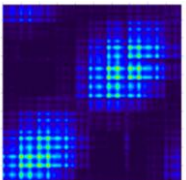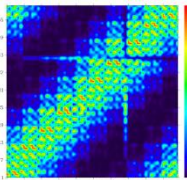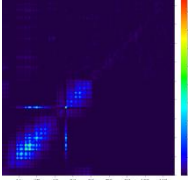
	C_{60}	[10]CPP		[10]CPP□C_{60}
λ	S_0-S_{38} (288 nm)	S_0-S_2 (314 nm)	S_0-S_{49} (193 nm)	S_0-S_{39} (313 nm)
E_{ge}	4.30 eV	3.92 eV	6.46	3.96 eV
	π-π^*	π-π^*(LE)	π-π^*+ICT	π-π^*
CDD				
TDM				
S_r	0.943 a.u.	0.888a.u.	0.858 a.u.	0.864 a.u.
D	0.001 Å	0.006 Å	0.468 Å	0.005 Å
H	3.848 Å	6.367 Å	6.477 Å	6.695 Å
t	-2.221 Å	-2.186 Å	-1.980 Å	-3.509 Å
HDI	2.96 a.u.	3.74 a.u.	3.93 a.u.	3.16 a.u.
EDI	2.99 a.u.	3.74 a.u.	2.94 a.u.	2.97 a.u.
E_c	3.68 eV	2.70 eV	2.61 eV	2.50 eV

Table S7. The wavelength (λ), transition energy (E_{ge}) charge density difference (CDD), transition density matrix (TDM), overlap of hole-electron index (Sr), The distance between the hole and the electron's center of mass index (D), The overall mean distribution width of electrons and holes index (H), the degree of hole and electron separation index (t), hole delocalization index (HDI), electron delocalization index (EDI), exciton binding energy (E_c) of the excited state corresponding to the main absorption peak of C_{60}, [11]CPP and [11]CPP☐C_{60}.
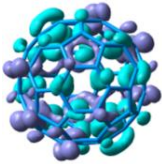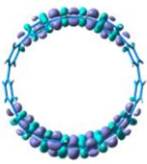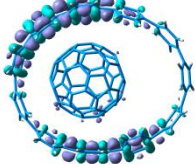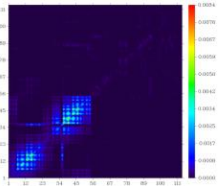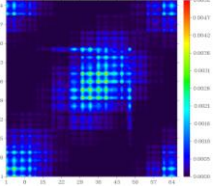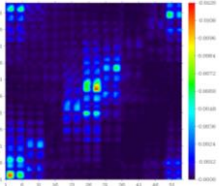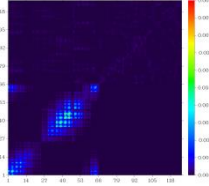
	C_{60}	[11]CPP		[11]CPP☐C_{60}
λ	S_0-S_{38} (288 nm)	S_0-S_2 (317 nm)	S_0-S_{45} (201 nm)	S_0-S_{39} (307 nm)
E_{ge}	4.30 eV	3.92 eV	6.17	4.03 eV
	π-π^*	π-π^*+ICT	π-π^*+ICT	π-π^*
CDD				
TDM				
S_r	0.943 a.u.	0.793 a.u.	0.790 a.u.	0.861 a.u.
D	0.001 Å	0.045 Å	0.125 Å	0.098 Å
H	3.848 Å	7.672 Å	7.783 Å	7.046 Å
t	-2.221 Å	-6.177 Å	-5.530 Å	-3.892 Å
HDI	2.96 a.u.	3.30 a.u.	2.14 a.u.	3.17 a.u.
EDI	2.99 a.u.	3.27 a.u.	2.19 a.u.	3.01 a.u.
E_c	3.68 eV	2.08 eV	1.52 eV	2.39 eV

Table S8. The wavelength (λ), transition energy (E_{ge}) charge density difference (CDD), transition density matrix (TDM), overlap of hole-electron index (Sr), The distance between the hole and the electron's center of mass index (D), The overall mean distribution width of electrons and holes index (H), the degree of hole and electron separation index (t), hole delocalization index (HDI), electron delocalization index (EDI), exciton binding energy (E_c) of the excited state corresponding to the main absorption peak of $Li^+@C_{60}$, [9]CPP and [9]CPP$\square$$Li^+@C_{60}$.
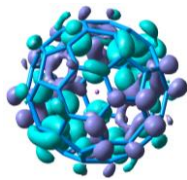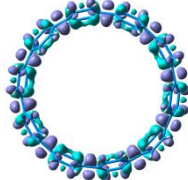
	$Li^+@C_{60}$	[9]CPP		[9]CPP$\square$$Li^+@C_{60}$
λ	S_0-S_{37} (288 nm)	S_0-S_2 (314 nm)	S_0-S_{49} (193 nm)	S_0-S_{32} (3.63 nm)
E_{ge}	4.30 eV	3.92 eV	6.46	3.64 eV
	π-π^*	π-π^*(LE)	π-π^{*+}ICT	π-π^{*}+IECT
CDD				
TDM				
S_r	0.943 a.u.	0.888 a.u.	0.858 a.u.	0.742 a.u.
D	0 Å	0.006 Å	0.468 Å	1.357 Å
H	3.852 Å	6.367 Å	6.477 Å	5.895 Å
t	-2.226 Å	-2.186 Å	-1.980 Å	-0.704 Å
HDI	2.96 a.u.	3.74 a.u.	3.93 a.u.	3.16 a.u.
EDI	2.95 a.u.	3.74 a.u.	2.94 a.u.	2.48 a.u.
E_c	3.67 eV	2.70 eV	2.61 eV	2.54 eV
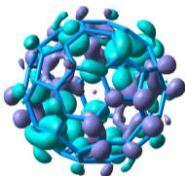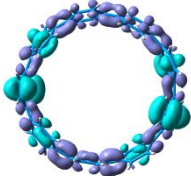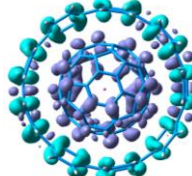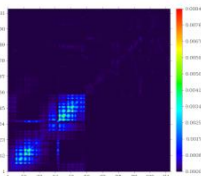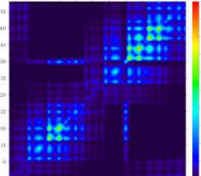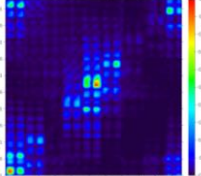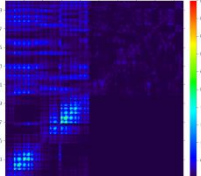
Table S9. The wavelength (λ), transition energy (E_{ge}) charge density difference (CDD), transition density matrix (TDM), overlap of hole-electron index (Sr), The distance between the hole and the electron's center of mass index (D), The overall mean distribution width of electrons and holes index (H), the degree of hole and electron separation index (t), hole delocalization index (HDI), electron delocalization index (EDI), exciton binding energy (E_c) of the excited state corresponding to the main absorption peak of $Li^+@C_{60}$, [10]CPP and [10]CPP□$Li^+@C_{60}$.
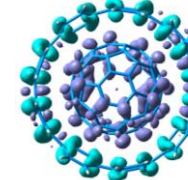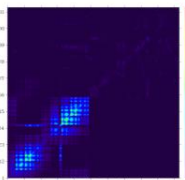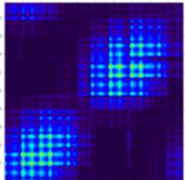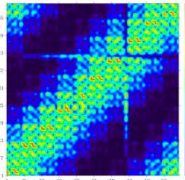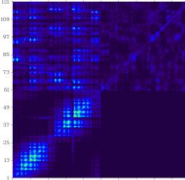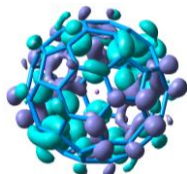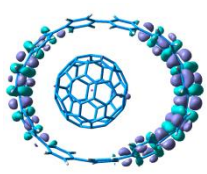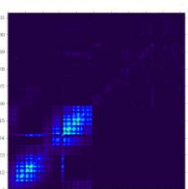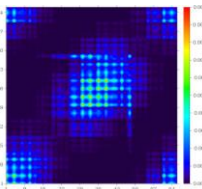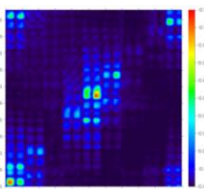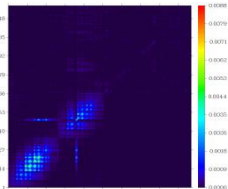
	$Li^+@C_{60}$	[10]CPP		[10]CPP□$Li^+@C_{60}$
λ	S_0-S_{37} (288 nm)	S_0-S_2 (314 nm)	S_0-S_{49} (193 nm)	S_0-S_{32} (323 nm)
E_{ge}	4.30 eV	3.92 eV	6.46	3.84 eV
CDD	π-π^*	π-π^*(LE)	π-π^*+ICT	ICT+IECT
TDM				
S_r	0.943 a.u.	0.888 a.u.	0.858 a.u.	0.778 a.u.
D	0 Å	0.006 Å	0.468 Å	0.001 Å
H	3.852 Å	6.367 Å	6.477 Å	6.167 Å
t	-2.226 Å	-2.186 Å	-1.980 Å	-4.071 Å
HDI	2.96 a.u.	3.74 a.u.	3.93 a.u.	2.91 a.u.
EDI	2.95 a.u.	3.74 a.u.	2.94 a.u.	2.38 a.u.
E_c	3.67 eV	2.70 eV	2.61 eV	2.55 eV

Table S10. The wavelength (λ), transition energy (E_{ge}) charge density difference (CDD), transition density matrix (TDM), overlap of hole-electron index (Sr), The distance between the hole and the electron's center of mass index (D), The overall mean distribution width of electrons and holes index (H), the degree of hole and electron separation index (t), hole delocalization index (HDI), electron delocalization index (EDI), exciton binding energy (E_c) of the excited state corresponding to the main absorption peak of $Li^+@C_{60}$, [11]CPP and [11]CPP□$Li^+@C_{60}$.

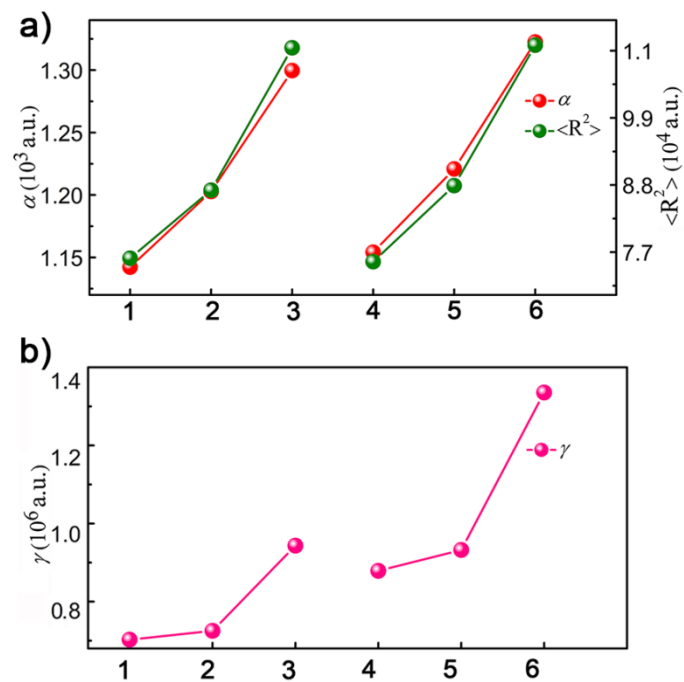|	$Li^+@C_{60}$	[11]CPP		[11]CPP□$Li^+@C_{60}$
λ	S_0-S_{37} (288 nm)	S_0-S_2 (317 nm)	S_0-S_{45} (201 nm)	S_0-S_{32} (324 nm)
E_{ge}	4.30 eV	3.92 eV	6.17	3.83 eV
	π-π^*	π-π^*+ICT	π-π^*+ICT	π-π^*(LE)
CDD				
TDM				
S_r	0.943 a.u.	0.793 a.u.	0.790 a.u.	0.855 a.u.
D	0 Å	0.045 Å	0.125 Å	0.054 Å
H	3.852 Å	7.672 Å	7.783 Å	7.550 Å
t	-2.226 Å	-6.177 Å	-5.530 Å	-5.804 Å
HDI	2.96 a.u.	3.30 a.u.	2.14 a.u.	3.38 a.u.
EDI	2.95 a.u.	3.27 a.u.	2.19 a.u.	3.14 a.u.
E_c	3.67 eV	2.08 eV	1.52 eV	2.35 eV

Figure S1. a) the α_{tot} and $<R^2>$ values for the complexes. b) The γ_{tot} values of the complexes calculated at BHandHLYP/6-31+G(d) level.
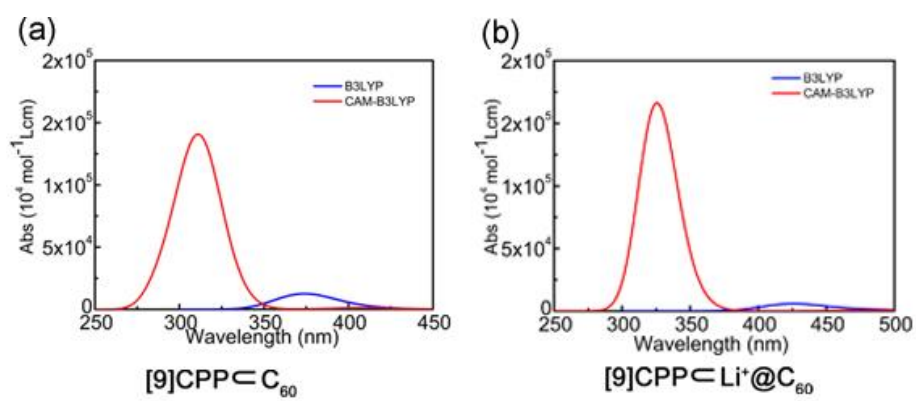
Figure S2. The theoretically simulated spectra of [9]CPP⊂C$_{60}$ (a) and [9]CPP⊂Li$^+$@C$_{60}$ (b) obtained at TD-B3LYP and TD-CAM-B3LYP in CH$_2$Cl$_2$.

Electron circular dichroism spectra of the complexes.

The circular dichroism of complex **1** contained two positive bands at 381.7 and 318.3 nm and two negative bands at 365.5 and 289.5 nm (Figure S3). For **2**, the circular dichroism contained one positive band at 318.8 nm and one negative band at 307.9 nm. The circular dichroism of **3** mainly contained one positive band at 311.9 nm. When lithium ions were embedded in fullerenes, the spectra were slightly redshifted. For **4**, its circular dichroism mainly contained two positive bands at 449.8 and 337.1 nm, which were redshifted by 68 nm with respect to that of **1**. The circular dichroism of **5** showed one negative band at 323.5 nm. The circular dichroism of **6** mainly contained two positive bands at 442.0 and 331.7 nm, as well as one negative band at 319.0 nm. It was suggested that the insertion of lithium ions into fullerenes contributed to the redshift of the circular dichroism spectra of the complexes.
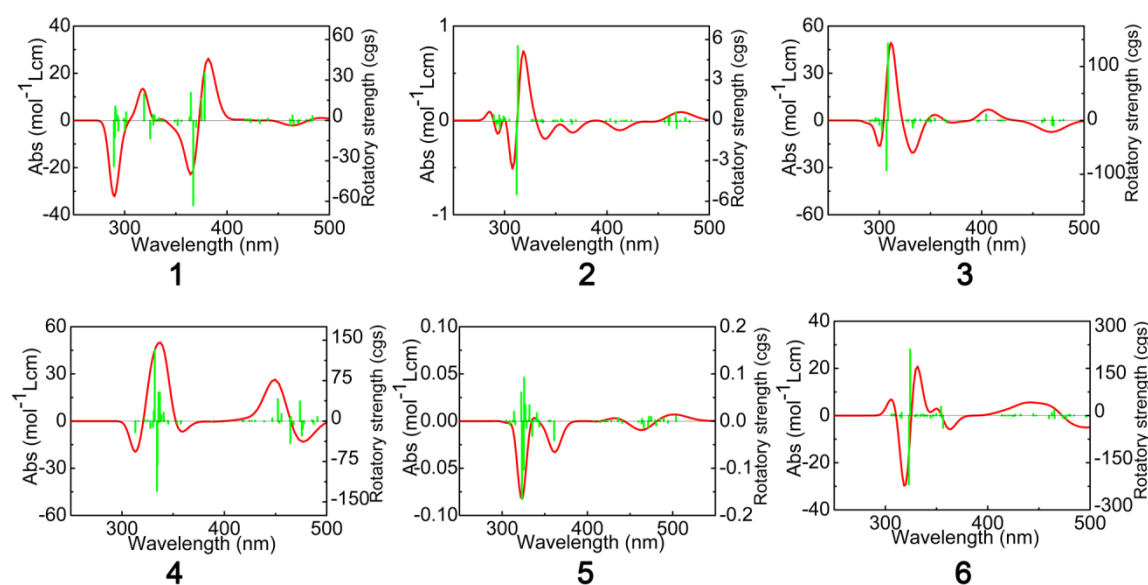

Figure S3. The circular dichroism (CD) spectra calculated at the TD-CAM-B3LYP/6-31G(d).

References

1. T. L. Bahers, C. Adamo, I. Ciofini. *J. Chem. Theory Comput.*, 2011, 7, 2498-2506.